1   # A critical study on impact damage simulation of

2   # IM7/8552 composite laminate plate

3   Hao Cui[a,b,1], Daniel Thomson[a], Sina Eskandari[a], Nik Petrinic[a]

4   *a Department of Engineering Science, University of Oxford, Oxford, United Kingdom*

5   *b School of Aerospace, Transport and Manufacturing, Cranfield University, Cranfield,*

6   *United Kingdom*

7   ## Keywords

9   ## Abstract

10   Plate impact tests on IM7/8552 composite laminates with different projectile

11   incident angles and velocities were carried out. Numerical simulations were conducted to

12   predict the impact damage, with both Puck and LaRC failure criteria having been employed in

13   this study. The dynamic failure performance of IM7/8552 lamina was reviewed first, by

14   referring to data obtained from experiments conducted at a range of strain rates. The

15   performance of the assessed modelling approaches was evaluated by comparing the results

16   of simulations against experimentally (quantitatively and qualitatively) acquired projectile

17   velocity, impact load and the failure modes of the plates. It proved to be challenging to model

---

[1]Corresponding author: hao.cui@cranfield.ac.uk

18   the macroscopic damage of the laminate at elevated projectile velocities; further

19   improvement can be made through enriching the dynamic material data and mitigating the

20   mismatch between the complex fibre architecture and its numerical representation.

21   1. Introduction

22   Composite fibre reinforced polymer composites have gained extensive application in

23   aerospace industry [1,2] and other industrial sectors including automotive [3] and civil

24   engineering [4]. These materials have shown superior mechanical performance compared

25   with metallic counterparts, thanks to their high stiffness and strength in the fibre direction.

26   Due to their anisotropic properties and the combination of fibre reinforcement and polymer

27   matrix, their failure modes have been found to be very complicated [5–7]. Many of these

28   composite structures may experience impact damage from different sources [8], such as bird

29   strike on aero-structures [9] and crashing of large vehicles [10]. Analysis and prediction of the

30   failure behaviour under impact loading then become vital in the design and certification of

31   such structures.

32   A lot of theories have been proposed for predicting the damage of composites, 19 of

33   them have been benchmarked during the World Wide Failure Exercise(WWFE) [11–13]. It was

34   concluded from this exercise that few of the current predictive failure theories were robust

35   enough for industrial applications. Some of these failure theories reflecting on the physical

36   failure mechanisms of composites, such as Puck's failure criteria[14,15], have shown

37   promising performance in some stress conditions. In recent years, several of these failure

38   criteria have been increasingly employed in predicting damage and fracture of composites,

39   including the dynamic failure process. The low velocity impact damage of composite

40   laminates have been mostly investigated, successful prediction from Puck's theory [16] have

41   been reported. The LaRC model [17] also uses a phenomenological approach to propose a

42   failure criteria specifically for fibre reinforced laminate composites. This model also may take

43   nonlinear matrix shear behaviour into account and it relates laminate configuration to ply

44   thickness and toughness [18], and its performance has been successfully demonstrated [19].

45   A continuum damage model has been proposed using these failure criteria [20,21]. Nonlinear

46   behaviour due to fibre rotation is also incorporated into the model by [22].

47   An exhaustive review of dynamic modelling work was not provided due to the scope

48   of the current paper, considering the fact that hundreds of papers per year being published

49   on the composites damage modelling [23]. Despite the increasing volume of failure theories

50   and numerical methodologies, our confidence in our composite modelling capability remains

51   to be confirmed due to the lack of systematic evaluation, such as the round-robin tests from

52   the WWFE [11–13]. It could be relatively easy to match some specific experiments with

53   numerical modelling, for example by tuning some damage parameters. However, it is not

54   conclusive to justify the validity of a modelling method if the input parameters were

55   calibrated against the same set of experiments, which the model is then used to reproduce.

56   The IM7/8552 has been one of the mostly studied composite material systems so far.

57 Various experiments have been reported on the ultimate strength in the fibre failure and the

58 inter-fibre failure modes, which are important input data for predicting the initiation of

59 damage, as highlighted in the previous WWFE[11–13].. The fracture toughness of different

60 failure modes, critical for analysing the growth and propagation of damage, have also been

61 studied extensively. On top of many studies in the quasi-static domain, it is worth noting that

62 considerable work is also available in dynamic regime. These accumulated data on the

63 IM7/8552 material have made it possible to calibrate strain rate-dependent models for

64 dynamic failure simulation, and arguably, the numerical simulation on this material may

65 represent state of the art capability in predicting dynamic failure of composites in general.

66   The aim of this paper is to provide a benchmark study on the dynamic damage

67 modelling of composites based on the Puck and LaRC failure criteria, using a bespoke impact

68 test on IM7/8552 composites. This work may help to highlight the performance and drawback

69 of current numerical methods, and provide insight on potential improvement in future. A

70 comprehensive survey of the properties of IM7/8552 laminates is provided as well, for

71 calibrating the material input cards of both models.

72
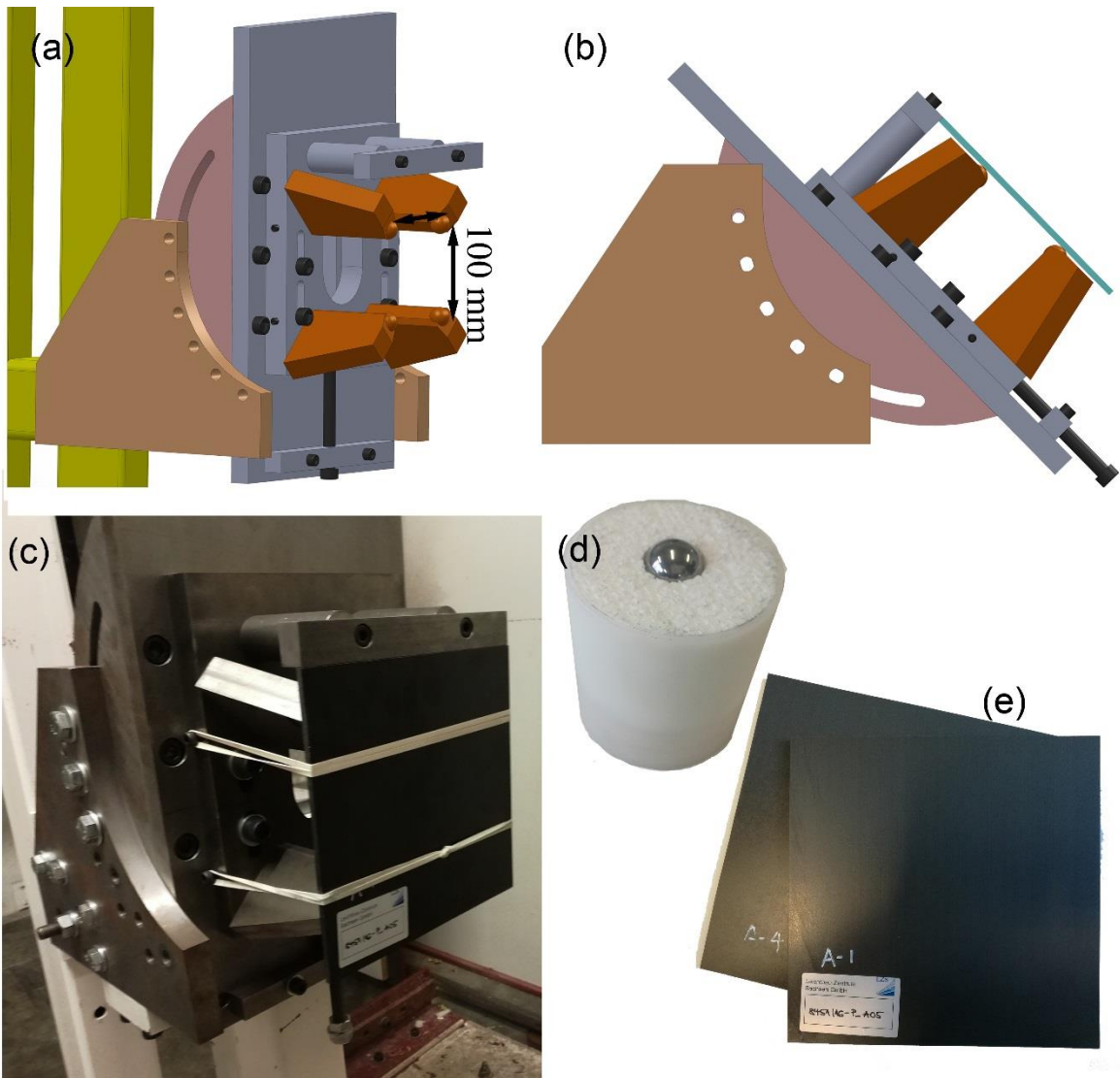
73   Fig.1 Plate impact setup,(a) the test configuration for 90°impact; (b) the configuration for

74   45°impact;(c) the actual test fixture with elastic band for holding the plate in place;(d) the

75   projectile(steel ball) in foam sabot; (e) the plate sample

2. Plate impact experiments

2.1 Material and sample

78   The samples were made with the IM7/8552 unidirectional prepregs, a detailed

79   introduction of the material will be given in Section 3.4. The layup was [0/45/90/-45]5s,

80 resulting in nominal thickness of 5mm. All panels have been checked with C-Scan to ensure

81 that good quality has been achieved with the manufacturing process, and then cut into the

82 size of 200*200mm using a diamond saw.

83 **2.2 Test setup**

84   The plate impact experiment in this section aims to investigate the failure mode of

85 composite panels under ballistic loading and provide detailed dataset for validating the

86 dynamic failure analysis. As shown in the Fig. 1, the panel was supported with 4 ball bearings

87 of 20 mm diameter. The space between these supporting balls is 100mm. Rubber bands were

88 used to hold the panel on the fixture. The constraint from these rubber bands can be safely

89 ignored due to their low moduli and strength. The fixture and sample holding was designed

90 in such a way that, it is very easy to be accurately simulated in a finite element environment,

91 avoiding complicated boundary conditions from traditional frame supports.

92   The plates were impacted with steel ball of 20mm diameter, the mass of these

93 projectiles was around 32.7 grams. The projectile was embedded in a foam sabot, and

94 accelerated to the required velocity using a 70 mm gas gun.

95   The composite plates were impacted at two different angles: 90° normal impact and

96 45° oblique impact; 10 tests were conducted for each angle. The impact velocity ranged from

97 21m/s up to 157 m/s, resulting in different combinations of failure modes.

2.3 Data process

99   A Photron high-speed camera was employed to capture the impact event. The digital

100   image correlation (DIC) method was used to analyse the displacement of the projectiles. The

101   velocity of the projectiles were then analysed from the change of displacement between

102   frames of image. The light curtain attached on the gun also provided the velocity of the

103   projectile, and it has been verified that the difference in velocity estimated between these

104   two methods was less than 5%.

105   It has been very challenging to record the impact force during these high velocity

106   impact events. In this work, only the displacement and velocity of the projectile was obtained

107   with reasonable accuracy and reliability, using the DIC method. The acceleration of balls were

108   calculated by further differentiation of the velocity history, which is smoothed with moving

109   averaging method. The impact load applied on the plates was the calculated as $F = a\,m$,

110   where a and m are the acceleration and mass of the projectile.

111   **Table 1 Elastic properties for IM7/8552 unidirectional composite**

E11	162095.8	Mpa
E11c	140928.9	Mpa
E22c	9721.61	Mpa
G12	4688.436	Mpa
v12	0.362	

3. Dynamic damage theory

112

113   For the two compared models, an orthotropic linear elastic behaviour is shared

114   among them, with the elastic properties listed in Table.1. The stiffness of the IM7/8552 is

115   considered as strain rate dependent in the LaRC model. The detailed damage models are

116   introduced as follows.

3.1 Puck failure criteria

117

118   For matrix or Inter-fibre fracture (IFF) a modified Puck failure criterion was used [24].

119   The original Puck criterion [14] is a Mohr-Coulomb based theory where a frictional, or

120   pressure-dependent, failure function, f_E, is evaluated on potential fracture planes transverse

121   to the fibre direction. A numerical search is required in order to determine the critical plane

122   where the failure function, f_E, is maximized. The failure function, or exposure because it

123   indicates the material proximity to failure, is evaluated by rotating the material stress state

124   onto the potential fracture plane (**Error! Reference source not found.**), where the shear

125   stresses, τ_{n1} and τ_{nt}, drive the onset of fracture and the normal stress, σ_n, can either promote

126   or impede this depending, respectively, on if it is tensile or compressive. Because of this,

127   Puck's criterion is given by two equations depending on the direction of the normal stress, σ_n.

128   The surface tractions on the Puck failure plane is calculated as:

129
$$\begin{bmatrix} \sigma_1 \\ \sigma_n \\ \sigma_t \\ \tau_{n1} \\ \tau_{nt} \\ \tau_{1t} \end{bmatrix} = \begin{bmatrix} 1 & 0 & 0 & 0 & 0 & 0 \\ 0 & c^2 & s^2 & 0 & 2sc & 0 \\ 0 & c^2 & s^2 & 0 & -2sc & 0 \\ 0 & 0 & 0 & c & 0 & s \\ 0 & -cs & cs & 0 & c^2 - s^2 & 0 \\ 0 & 0 & 0 & -s & 0 & c \end{bmatrix} \cdot \begin{bmatrix} \sigma_{11} \\ \sigma_{22} \\ \sigma_{33} \\ \tau_{12} \\ \tau_{23} \\ \tau_{13} \end{bmatrix}$$
(1)

130 where $c = \cos(\theta)$ and $s = \sin(\theta)$.
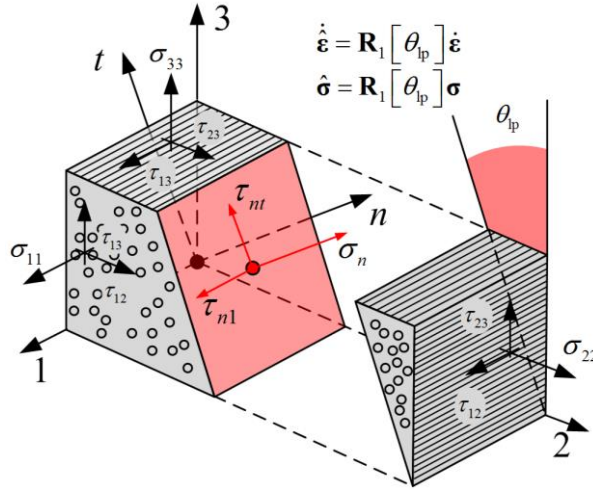
131

132 Fig.2. Schematic view of the rotation performed to transform the stresses into the IFF plane.

133 The stress exposure, f_E, given below, indicates the proximity of the material to IFF-

134 type failure on the considered potential fracture plane with a value ranging from 0, unloaded

135 material, to 1, failure initiation [14,25].

136
$$f_E = \begin{cases} \sqrt{(1-p_t)^2 \left(\frac{\sigma_n}{Y_T}\right)^2 + \left(\frac{\tau_{n1}}{R_{n1}}\right)^2 + \left(\frac{\tau_{nt}}{R_{nt}}\right)^2} + p_t \frac{\sigma_n}{Y_T} \geq 1 \text{ for } \sigma_n \geq 0 \\ \sqrt{\left(p_c \frac{\sigma_n}{Y_C}\right)^2 + \left(\frac{\tau_{n1}}{R_{n1}}\right)^2 + \left(\frac{\tau_{nt}}{R_{nt}}\right)^2} + p_c \frac{\sigma_n}{Y_C} \geq 1 \text{ for } \sigma_n < 0 \end{cases}$$
(2)

137 where p_t, p_c and internal friction parameters [15], Y_T is the transverse tensile strength, Y_C is

138 the transverse tensile strength. R_{n1} is the in-plane shear strength, R_{nt} is calculated as [26]:

139 $$R_{nt} = Y_C \cos^2 \theta_{fr}^0 \qquad\qquad (3)$$

140 where θ_{fr}^0 is the failure angle in transverse compression tests[27].

141   After failure is predicted using the above criterion, a bilinear cohesive law is used of

142 the type described in [28,29], illustrated in **Error! Reference source not found.**, to damage

143 the tractions on the fracture plane, σ_n, τ_{n1} and τ_{nt}. In tis formulation, a damage variable D is

144 defined to produce linear softening in the effective stress vs effective displacement space,

145 $\sigma_{eff} - \delta$, from the point of initiation, δ_0, to final failure, δ_C:

146 $$D = \max\left\{0, \min\left\{1, \frac{\delta_C(\delta - \delta_0)}{\delta(\delta_C - \delta_0)}\right\}\right\} \qquad\qquad (4)$$

147   With the effective displacements, δ, obtained from the effective strain and

148 characteristic element length, l_c, introduced to alleviate the mesh dependency problem of
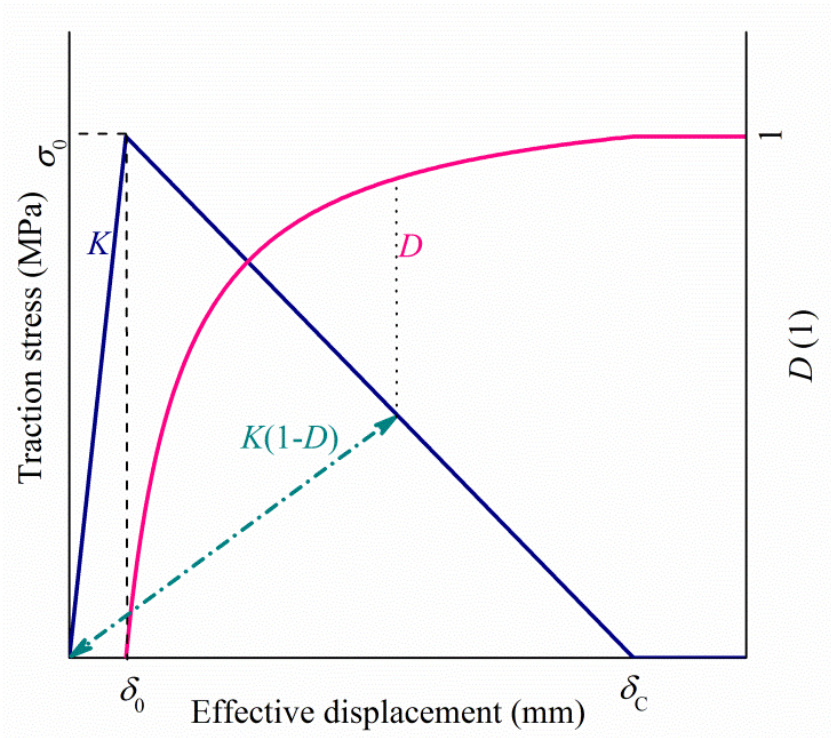
149 continuum damage modelling [18,19]:

150 $$\delta = l_c \varepsilon_{eff} \qquad\qquad (5)$$

151 and the displacement at failure calculated from the mixed mode fracture toughness, G_T:

152 $$\delta_C = \frac{2G_T}{\sigma_{eff}^C} \qquad\qquad (6)$$

153 $$G_T = \begin{cases} \dfrac{G_{IC}G_{IIC}(1+\eta^2\lambda)}{G_{IIC}+G_{IC}\eta^2\lambda}, & \gamma_{eff} \neq 0 \\ G_{IIC}, & \gamma_{eff} = 0 \end{cases} \qquad\qquad (7)$$

154

Fig.3. Damage evolution at Puck failure plane

155

156

157   The material may fail in the fibre direction under tension and compression load,

158 which is predicted here by maximum stress criteria. The continuum stiffness degradation will

159 start once the failure criteria is satisfied, which is controlled in a similar way as shown in Fig.3,

160 where the fibre fracture toughness equal to the area under the damage evolution curve.

161   Finally, fully-damaged elements, identified by the damage variable for any of the

162 failure modes reaching a limit of 0.999, are deleted to avoid numerical instabilities and allow

163 full perforation of the plate.

3.2 LaRC failure criteria and Maimi damage model

164

165   The LaRC is a set of six phenomenological failure criteria with the assumption of plane

166 stress conditions. LaRC uses *in situ* strength for evaluation of failure which depends on where

167 the ply is situated in the laminate, the number of plies bundled together, and the orientation

168 of the fibers in outer plies. *In situ* properties are calculated based on crack propagation in a

169 constrained ply. LaRC criterion for matrix failure under transverse tension reads:

170 $(1-g)\frac{\sigma_{22}}{Y_{T,is}} + g(\frac{\sigma_{22}}{Y_{T,is}})^2 + g(\frac{\tau_{12}}{R_{12,is}})^2 \leq 1$ (8)

171 Where $g = \frac{G_{IC}}{G_{IIC}}$ and "*is*" subscript represents *in situ* property. The criterion for matrix failure

172 under compression is:

173 $(\frac{\tau_{eff}}{R_{nt}})^2 + g(\frac{\tau_{eff}}{R_{n1,is}})^2 \leq 1$ (9)

174 Where the subscript "*eff*" means the stress components acting in fracture plane which is

175 calculated according to Eq(1). The transverse shear strength R_{nt} for LaRC model is calculated

176 as:

177 $R_{nt} = Y_C \cos(\theta_{fr}^0) \left[\sin(\theta_{fr}^0) + \frac{\cos(\theta_{fr}^0)}{\tan(2\theta_{fr}^0)} \right]$ (10)

178   For failure in fibre compression, the initial misalignment in the fibres is calculated

179 and, based on that, the effective stresses are derived. The effective stresses then contribute

180 to Mohr-Coulomb criterion, where, in the presence of compressive transverse loading, it

181 reads:

182    $\langle \frac{|\tau^{\,m}_{\,12}|+\eta^L \sigma^m_{22}}{R_{n1,is}} \rangle \leq 1$ (11)

183   And in the presence of tensile and transverse loading, the LaRC criterion reads:

184    $(1-g)\frac{\sigma^m_{22}}{Y_{T,is}} + g(\frac{\sigma^m_{22}}{Y_{T,is}})^2 + g(\frac{\tau^m_{12}}{R_{12,is}})^2 \leq 1$ (12)

185   In Eq (11, 12), the superscript "m" means the stress in the local coordinate with consideration

186   of fibre misalignment. Detailed information can be found in [18]. The maximum stress criteria

187   have been used for fibre tension failure prediction, similar to the previous Puck model.

188   The damage evolution is triggered once any failure criterion is reached, and the

189   degradation of stiffness is determined based on the energy dissipation per volume, similar to

190   what was introduced in previous section. All of damage parameters are scalar and evolve

191   linearly, but the damage parameter in fibre direction which evolves exponentially after fibre

192   pull-out. The details of the model is discussed in [21] and [30]. Element erosion is applied to

193   prevent instability. This criterion deletes an element when any damage variable reaches

194   0.999.

195   **3.3 Numerical plate impact model**

196   A numerical model has been built to simulate the plate impact experiments in Ls-

197   Dyna environment. The plate was modelled with 3 dimensional solid elements as shown in

198   Fig.4. The element size was 1x1x0.125 mm^3, one element per ply through-thickness. This

199   paper aims to evaluate the performance of these numerical models with the given mesh size.

200 It is expected that simulation accuracy will improve with finer mesh, however, it may be less

201 practical for industrial application. Two different user subroutines have been prepared

202 accordingly for both of the damage theories introduced in Section 2, representing the elastic

203 deformation and damage of the IM7/8552 laminates. The delamination is considered as a

204 special case of inter-fibre failure, and is simulated here with Puck and LaRC in bulk elements.

205 The supports and projectile were modelled as rigid bodies with a 3D solid mesh of

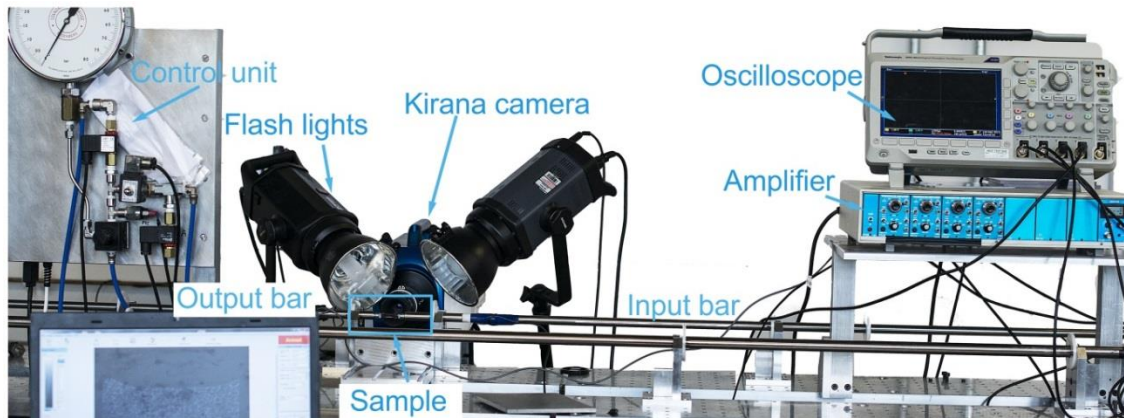206 approximately 2mm in length.
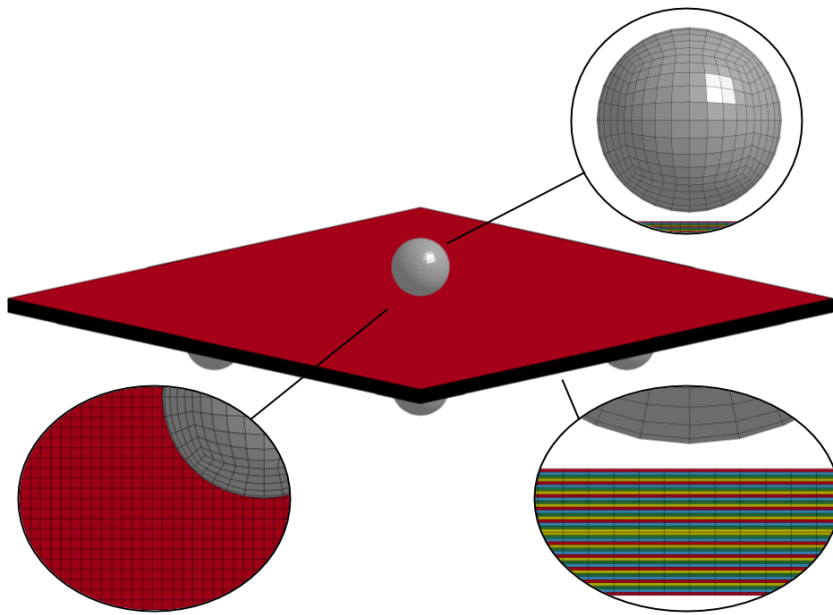
207

208   Fig.4. Simple 200x200x40 element mesh of the impacted plate, one element per ply

209   through-thickness, with supports and projectile modelled as rigid solids.

210 ## 3.4 Rate-dependent mechanical properties of IM7/8552

211

212   Fig.5. Split Hopkinson bar test system

213   The IM7/8552 material has been characterized at different strain rates with various

214 combinations of stress conditions, including considerable dynamic studies using the split

215 Hopkinson bar test system, one example for which is shown in Fig.4. The material

216 characterization will not be introduced in this work, instead detailed information of some

217 experiments can be found in recent publications of the authors[24,31–33]. These experiments,

218 in combination with work from peers   [34–37], resulted in an relatively complete datasheet

219 representing the rate-dependent failure envelope of IM7/8552 laminate. A summary of all

220 material data used in this simulation has been presented in Table.2.

221 **Table.2 Summary of IM7/8552 strength and fracture toughness data**

Property	Value	Test configuration	Strain rate	References
S_{11}(tension)	2625 MPa	Uniaxial tension	QS	[38]
S_{11}(Compression)	1451 MPa	Uniaxial compression	4e-4 s^{-1}	[34]
S_{11}(Compression)	2008 MPa	Uniaxial compression	119 s^{-1}	[34]
S_{22}(Tension)	60.2 MPa	Uniaxial tension	1e-4 s^{-1}	[39]

S_{22}(Tension)	113.3 MPa	Uniaxial tension	300 s^{-1}	[39]
S_{22}(Compression)	400.6 MPa	Uniaxial compression	5e-4 s^{-1}	[32]
S_{22}(Compression)	248.7 MPa	Uniaxial compression	300 s^{-1}	[39]
S_{12}	112.7 MPa	±45° laminates tension	5e-4 s^{-1}	[31]
S_{12}	149.7 MPa	±45° laminates tension	1300 s^{-1}	[31]
G_{IC}	0.22 N/mm	Double cantilever beam	Quasi-static	[40]
GIC	0.2 N/mm	Dynamic wedge opened double cantilever beam	Dynamic	[41]
G_{IIC}	0.66 N/mm	End notched flexure	Quasi-static	[42]
G_{IIC}	0.922 N/mm	End notched flexure	Dynamic	[42]
G_{FT}	82.0 N/mm	Compact tension	Quasi-static	[33]
G_{FT}	195.8 N/mm	Compact tension	Dynamic	[33]
G_{FC}	101.6 N/mm	Compact compression	Quasi-static	[43]
G_{FC}	165.6 N/mm	Compact compression	Dynamic	[43]

Here S11 is the longitudinal strength, S22 is the transverse strength, S12 is the in-plane shear strength. GIC is the mode I delamination fracture toughness, GIIC is the mode II delamination fracture toughness, GFT is the fracture toughness in fibre tension mode, G_{FC} is the fracture toughness in fibre compression mode

222   The longitudinal tensile strength, obtained from tension tests of the 0° plate, has

223   recently been reported to be dependent on the through-thickness compression stress[44] but

224   this effect was not taken into consideration. In addition, diverse data has been observed in

225   the longitudinal compression strength and there could be more than 50% difference in the

226   strength measured, depending on the specimen geometry and test methods [36,45,46]. The

227   transverse tension strength is also very difficult to measure, as it could be largely affected by

228   surface treatment and boundary conditions [43], and the data reported in this paper is lower

229   than data available in literature [43,47]. The mode I delamination fracture toughness is fairly

230   constant across thr literature, however, the mode II delamination toughness shows significant

231   variation [48], and could also be dependent on the transverse stress [49]. Finally, fracture

232   toughness tests in the fibre failure mode are limited and pioneering work from Pinho et.al [50]

233   suggest 20% difference in the fracture toughness from the value listed in above.

234   In the simulation with Puck's failure criteria, the material input card was filled with

235   those parameters tested at high strain rate wherever available. In the LaRC damage model, a

236   rate-dependent model has been introduced for representing the gradual change of material

237   parameters with respect to the strain rate of each individual element. There is a limit of

238     $300 s^{-1}$ for strain rate for stability after which the parameters will not vary anymoreIn

239   addition to strain-rate damping. These viscoelastic parameters are obtained based on

240   experiments by [51]. Elastic properties are calculated based on:

241     $$f_e(\dot{\varepsilon}) = (k_e \dot{\varepsilon})^{\frac{1}{n_e}}, \ k_e = 1.60 \times 10^{-4}, n_e = 2 \tag{11}$$

242   Strength properties are also updated with local strain rate:

243     $$f_e(\dot{\varepsilon}) = (k_u \dot{\varepsilon})^{\frac{1}{n_u}}, k_u = 1.13 \times 10^{-4}, n_u = 4 \tag{12}$$

244   4. Results from experiments and simulations

245   There were 20 experiments on the composite plates at velocities ranged from 20m/s

246   to 157 m/s. It has been observed that matrix dominated failure including delamination is the

247   major failure mode in low and medium velocity impact; more fibre rupture and splitting was

248   noticed as the increase of impact velocity. Therefore, four testing cases have been simulated

249   in the paper for a comprehensive evaluation of these numerical models in capturing different

250   failure modes Each of the testing case is introduced in a separate section as following.
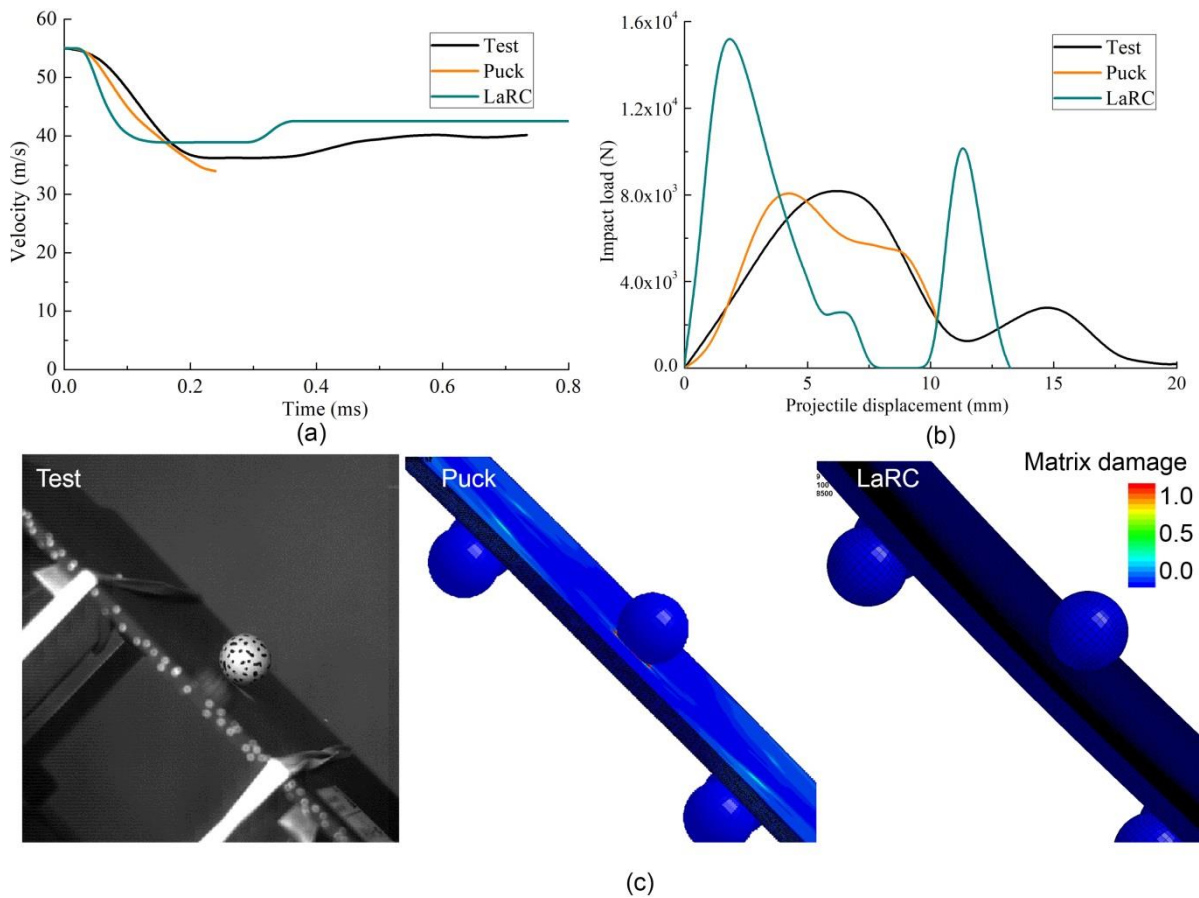
251   **4.1 90 degree impact at 59m/s**
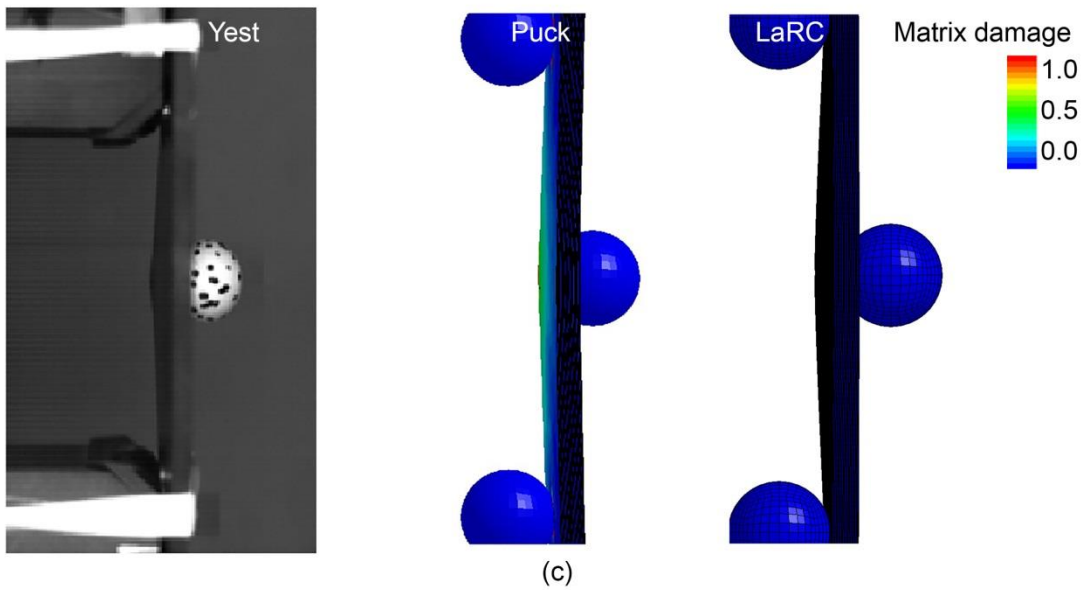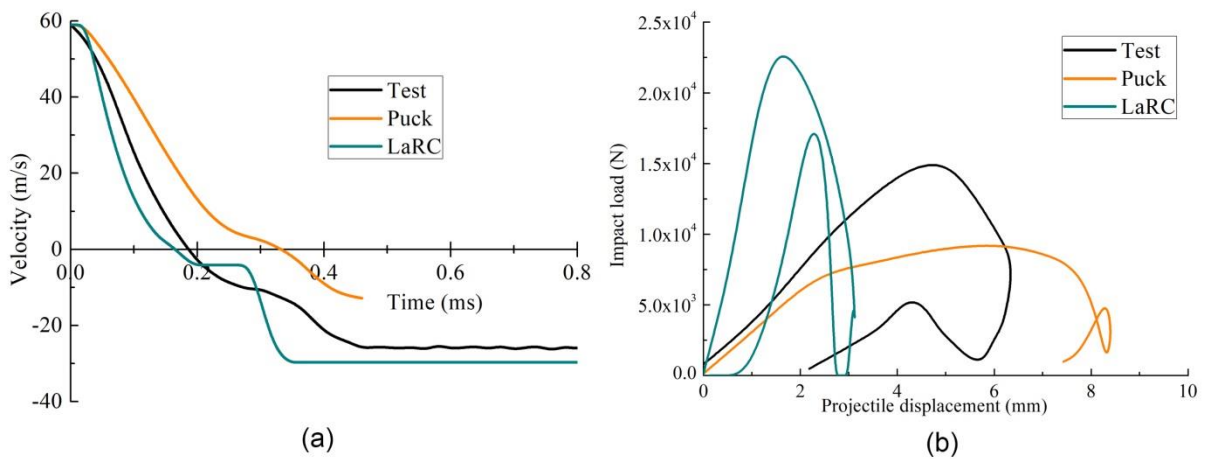
252

253   Fig.6 90° plate impact response at velocity of 59m/s from experiment and simulations: (a)

254   the velocity history during impact; (b) the Impact load-projectile displacement curves(c)

255   comparison of failure modes.

256   The plate tested at 90° with projectile of 59 m/s has been selected for modelling. The

257   global deformation and failure modes from simulations and experiments look very similar

258   among each other as shown in Fig.6c. At this level of impact velocity, matrix dominated inter-

259   fibre failure, including delamination, has been the major failure mode, although not clearly

260   visible from the high-speed camera image here. The deformation of plates have been

261   successfully captured in both Puck and LaRC model.

262   The projectile velocity from simulations and test has been summarized in Fig.6a,

263   where the velocity value changed from positive to negative due to the bouncing back of the

264   projectile. The simulation with Puck didn't capture the full impact event, due to excessive

265   distortion of damaged element that killed the time increment. The LaRC model provided good

266   prediction of the velocity history, the plateau during bouncing back process was due to the

267   vibration of plate that makes it lose contact with projectile, a similar step on experimental

268   curve is also noticeable.

269   The impact load from simulations have been calculated by the acceleration data of

270   projectile, and plotted with experimental results in Fig.6b. The Puck model underestimated

271   the peak contact load during, and the maximum displacement from this simulation was longer

272   than experimental data. The LaRC seemed to overestimate the peak force, and the raising

273   edge of the force-displacement curve is steeper than the other two. The strain rate dependent

274   modulus of LaRC model should be responsible for the artificially increase stiffness of the plate.

4.2 45 degree impact at 55m/s

(a)

(b)

(c)

Fig.7 45° plate impact response at velocity of 55m/s from experiment and simulations: (a)

the velocity history during impact; (b) the Impact load-projectile displacement curves(c)

comparison of failure modes.

The result from plate impact at 45° with projectile velocity of 55m/s is shown in Fig.7.

The Puck modelling was terminated after the project lose contract with plate, as element

distortion have resulted in significantly reduction of time increment in these simulations.

There is not much visible damage from the surface of plate as suggested by Fig.7c. all

simulations have reproduced such failure mode, however, the damage index near supporting

balls suggests that inter-fibre damage is likely to happen at these four corners as well. The

286   velocity profiles from both simulations and the experiments agree with each other quite well,

287   indicated that the energy dissipation was also of similar level among them. The Impact load

288   has been nicely reproduced by Puck model, however, the LaRC model have predicted much

289   higher peak load than experimental data.
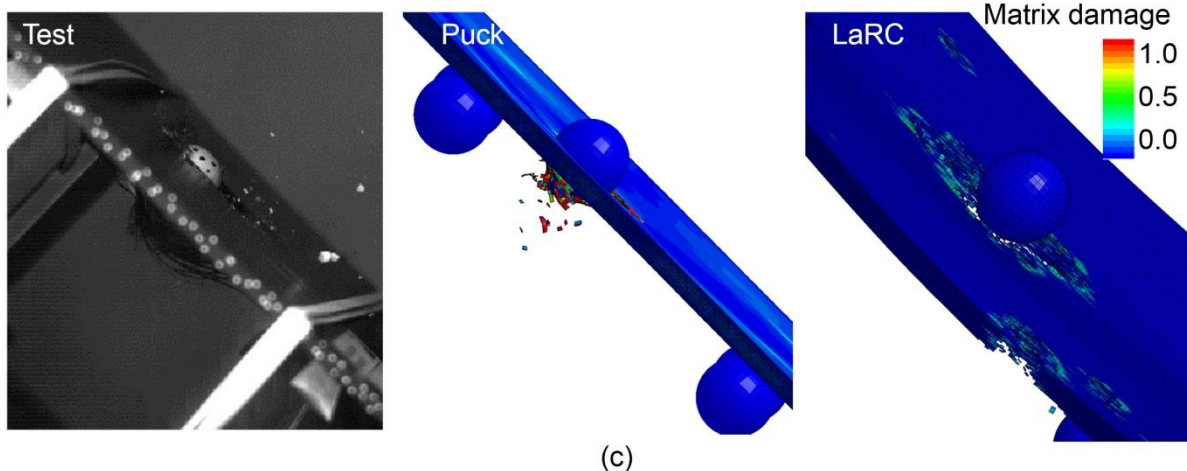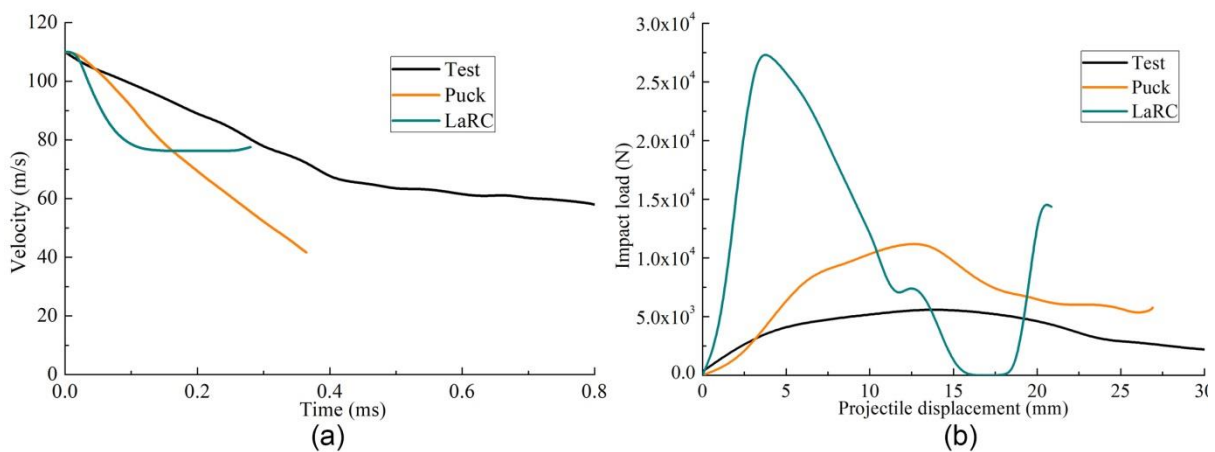
290   **4.3 90 degree impact at 106 m/s**
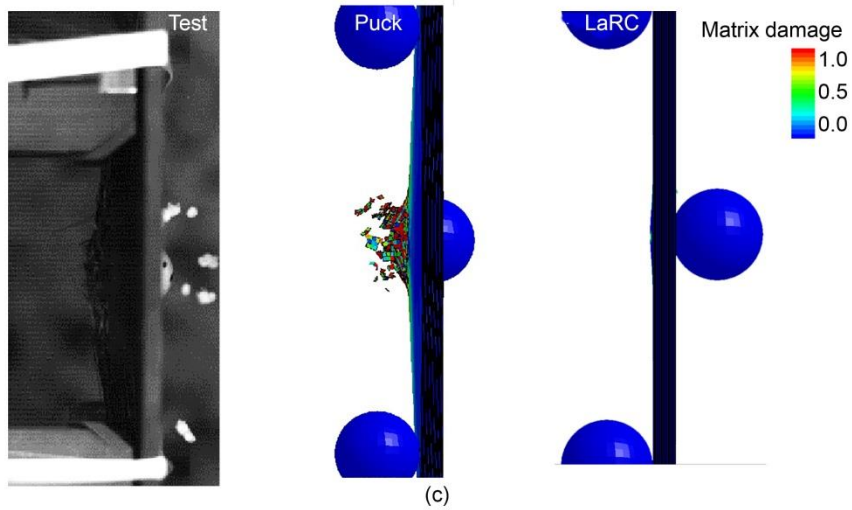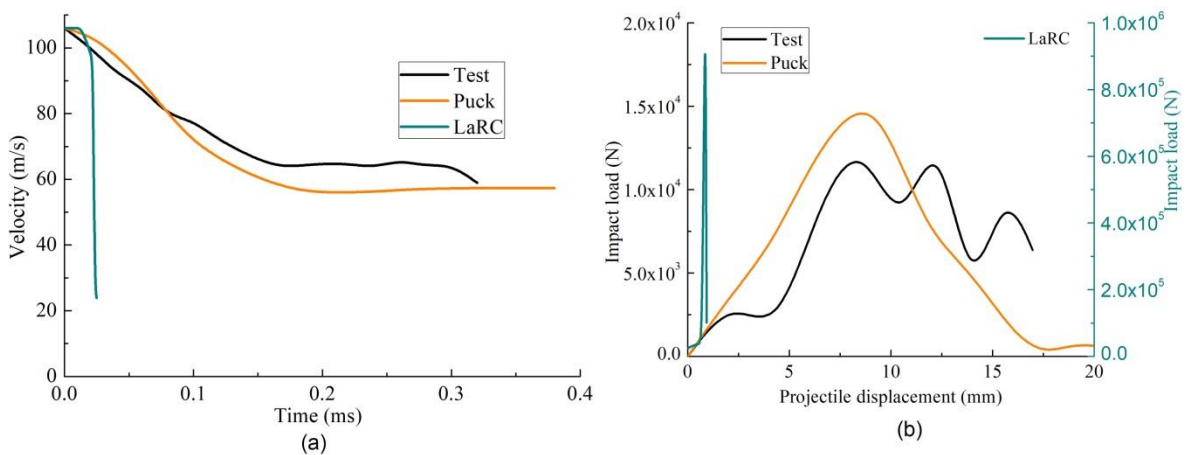
291

292   Fig.8 90° plate impact response at velocity of 106m/s from experiment and simulations: (a)

293   the velocity history during impact; (b) the Impact load-projectile displacement curves (c)

294   comparison of failure modes.

295   There is more damage occurring as the increase of impact velocity, as shown in Fig.8c,

296   and the plate has been penetrated with the projectile in test, with considerable fibre splitting

297   and rupturing. Such failure mode was captured by the Puck failure model, although the

298   damage is largely in the format of fragmentation, rather than the splitting of continuum fibres

299   in test. The velocity of projectile was properly predicted with the Puck model, while LaRC

300   model resulted in very rapid decrease of velocity as shown in Fig.8a. This rapid decrease was

301   correlated to the unusually high impact load as shown in Fig.8b.

302   **4.4 45 degree impact at 106m/s**


(a)

(b)

(c)

303

304　　　Fig.9 45° plate impact response at velocity of 110m/s from experiment and simulations: (a)

305　　　the velocity history during impact; (b) the Impact load-projectile displacement curves;(c)

306　　　　　　　　　　　　　　　　comparison of failure modes.

307　　　　　　The comparison between experiment and simulation of 45° plate impacted at

308　　　110m/s is shown in Fig.9. The penetration damage to plate has been successfully predicted

309　　　by both models. The Puck model seemed to provide better match with experiment than the

310　　　LaRC model, as excessive element deletion was noticed from the later one. The velocity

311　　　history from both simulations show noticeable deviation from the test result. Both models

312　　　also overestimated the impact load as well.

313　　　**4.5 Energy absorption**
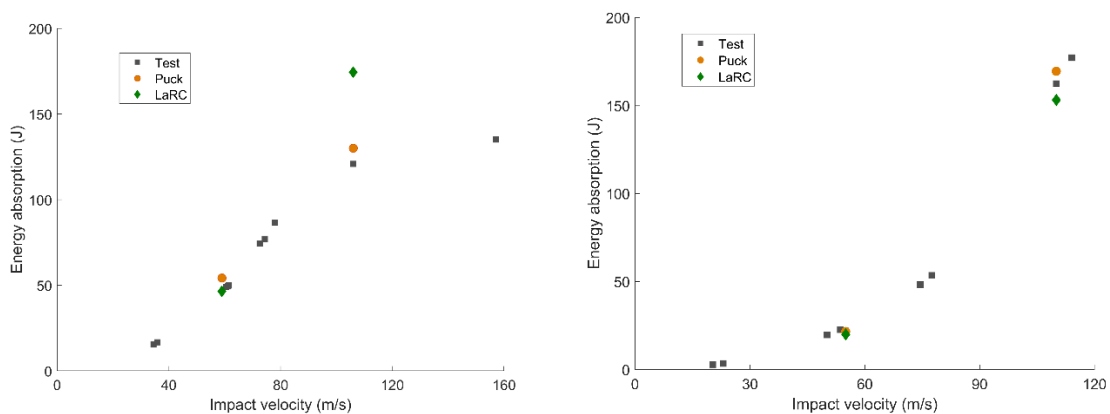
314

315　　　Fig.10. Energy dissipation from experiments and simulations,(a) 90°impact and (b)45°impact

316　　　　　　The energy being absorbed during the impact damage of the plate was calculated by

317　　　the difference of projectile kinetic energy before and after the event. There was rigid

318　　　movement and vibration of plates excited during the event that also consumed some of the

319   projectile kinetic energy, therefore, the energy absorption shown in Fig.10a is higher than

320   actual energy dissipated during damage process. In the 90° impact tests, the energy

321   absorption increased with the projectile velocity, which then plateaued due to the

322   penetration of plate. In the 45° impact, the energy absorbed by plate kept increasing within

323   the tested range of velocity. The simulations from both models have reproduced the energy

324   dissipation performance reasonably well.

325   ## 5. Discussions

326   An effort has been made here for benchmarking the dynamic modelling capacities

327   on some popular numerical models. It is worth emphasising that, this study shouldn't indicate

328   the level of accuracy of each damage theory, i.e. Puck and LaRC. Rather, this shows the

329   performance of the complete dynamic simulation settings, including also the way of

330   interpreting rate-dependent material data, mass scaling and element erosion etc.   Each

331   single setting listed above can have predominant effect on the simulation. In addition, these

332   models were both calibrated with coupon scale tests at two different strain-rate regions

333   (dynamic and quasi-static) and then used directly to model the experiments at the component

334   scale and a range of different impact velocities with no further calibration or fitting of the

335   input parameters. This served to demonstrate a reliable validation of composite modelling

336   capabilities without re-calibration and curve fitting, which has been standard practice in the

337   past. A collection of benchmark tests at different velocities and impact angles, such as the

338   ones presented here, will be critical to validate any developments in this area.

339   The discussion that follows is meant to evaluate the performance of current

340   modelling capabilities, which can be fitted to produce good results for a specific test but found

341   challenging to reproduce a broader range of loading scenarios.

342   For the Puck model, the high strain-rate material data was used and, overall,

343   performed reasonably well in current study, with the impact load and energy dissipation

344   being reproduced with acceptable accuracy. In the LaRC model, on the other hand, both the

345   stiffness and strength were considered as strain rate dependent. However, without tuning

346   these rate-dependent coefficients, the stiffness and peak impact load were overestimated.

347   Technically, rate-dependent material data should be more versatile for modelling dynamic

348   damage process, as the local strain rate keeps changing and is different from one location to

349   another. However, proper calibration of this effect, so as to get a reliable estimation of strain

350   rate for each element, can be very challenging without additional curve fitting to match the

351   experimental result and avoid any overshoots as shown in this work.

352   Another issue observed during this exercise had to do with numerical instabilities

353   due to distortion and failure. Elements may get distorted once the stiffness degradation was

354   triggered by reaching certain failure criteria. Such distortion is highly likely for the inter-fibre

355   failure of Puck theory, which may result in an inclined failure plane in the element with an

356   angle against the loading axis. The distorted elements will reduce the computational time

357   increment, and eventually result in abortion of the simulation, as shown in some of the Puck

358   simulations. Mass scaling can mitigate this issue to some extent, however, its effect is limited

359   as extensive application can artificially increase the whole mass of the model and affect the

360   accuracy of simulation. Similarly, erosion of distorted element may also resulted in lower

361   model mass than reality and severely affect the contact force in the simulation, as was

362   observed for the Puck model at lower velocity impacts in particular.

363   The failure of the plate at medium rate impact was dominated by inter-fibre failure,

364   including delamination. Although cohesive element has been traditionally used for

365   delamination prediction, the Puck and LaRC models that account for general inter-fibre failure,

366   appear to be successful for such simulations. Considering the fact that interface elements

367   normally require high computational effort, continuum damage models with inter-fibre

368   damage within the bulk element can be an efficient alternative solution, especially for

369   engineering applications.

370   The 45° impact test proves extremely useful validation case as it adds complexity to

371   delamination and ply failure with respect to the 90deg impact case. As seen in the numerical

372   results, one same model can produce reasonably good results in the simpler 90° case but fail

373   to match the 45° impact. In addition, in industrial applications impact is unlikely to occur

374 perfectly normal to a flat plate, instead being more likely to occur on oblique or curved

375 components. The normal velocity to the plate surface in this case, around 78 m/s, was close

376 to the ballistic limit, which makes it significantly more challenging to model. Because of this,

377 a minor under- or overestimation of material properties can result full, partial, or even no

378 perforation, as observed with the difference between the two models compared in section

379 4.4 – the LaRC based model over-predicted the extent of damage while in the Puck-based

380 model it was under-predicted.

381   In general, as expected, the numerical models have shown successful prediction of

382 certain test cases, while, failing to match the experiments in others. The velocity history has

383 been found to be relatively easy to reproduce among those experimental data acquired, while

384 the impact load can be very challenging to predict. The complicated plate perforation damage

385 wasn't successfully simulated, probably because of the continuous fibre architecture that

386 cannot be represented by current continuum bulk element. For example, the in-plane shear

387 normally results in splitting of fibres, while there is no distinction between it and the

388 transverse shear rupture of fibres. Novel numerical modelling methodologies are needed to

389 physically represent the microstructures of composites and its corresponding anisotropic

390 failure modes.

391   A comprehensive understanding of the dynamic damage mechanisms of composites

392 and their evolution with changes in strain-rate will help to provide accurate input data for the

393   numerical modelling. The IM7/8552 material was one of the most investigated materials, with

394   all dynamic data summarized in Table.2. However, there is still many data missing at dynamic

395   rates, and more experiments in this field are certainly encouraged, as a properly calibrated

396   rate-dependent model of the material properties is key to enhance dynamic modelling

397   capabilities in the future.

398   ## 6. Conclusions

399   Plate impact tests have been carried out at two different incidence angles with

400   projectiles of various velocities. The IM7/8552 material was used for making these plates, and

401   the literature survey have been done for its dynamic failure properties.

402   Numerical models have been developed for predicting the impact damage, where

403   Puck and LaRC failure criteria have been implemented separately for the inter-fibre failure

404   damage.

405   These models have been successfully used in the past to reproduce coupon-level

406   experiments at certain strain rates, however a proper rate-dependent validation at larger

407   scales has proven challenging without further tuning of material parameters.

408   The comparison between numerical simulation and experiments showed that,

409   projectile velocity is relatively easy to predict, while the force-displacement curves are

410   challenging to reproduce. There is also deviation between the actual failure modes and

411 numerical prediction, largely due to the mismatch between the complex fibre architecture

412 and its numerical representation.

413   Comprehensive characterization of the material response at dynamic loading rate

414 will contribute to improved dynamic modelling capabilities and avoid the need for curve

415 fitting in order to produce accurate large scale dynamic results.

References

417 [1]   GE tests GE9X composite fan blades, Reinf. Plast. (2014) 5. doi:10.1016/S0034-

418   3617(13)70162-0.

419 [2]   M. Nishikawa, K. Hemmi, N. Takeda, Finite-element simulation for modeling composite

420   plates subjected to soft-body, high-velocity impact for application to bird-strike

421   problem of composite fan blades, Compos. Struct. 93 (2011) 1416–1423.

422   doi:10.1016/j.compstruct.2010.11.012.

423 [3]   P. Feraboli, A. Masini, Development of carbon / epoxy structural components for a high

424   performance vehicle, Compos. Part B. 35 (2004) 323–330.

425   doi:10.1016/j.compositesb.2003.11.010.

426 [4]   J.G. Teng, T. Yu, D. Fernando, Strengthening of steel structures with fiber-reinforced

427   polymer composites, J. Constr. Steel Res. Rev. 78 (2012) 131–143.

428   doi:10.1016/j.jcsr.2012.06.011.

429 [5] A.E. Scott, M. Mavrogordato, P. Wright, I. Sinclair, S.M. Spearing, In situ fibre fracture

430 measurement in carbon − epoxy laminates using high resolution computed

431 tomography, Compos. Sci. Technol. 71 (2011) 1471–1477.

432 doi:10.1016/j.compscitech.2011.06.004.

433 [6] S.C. Garcea, I. Sinclair, S.M. Spearing, P.J. Withers, Mapping fibre failure in situ in

434 carbon fibre reinforced polymers by fast synchrotron X-ray computed tomography,

435 Compos. Sci. Technol. 149 (2018) 81–89. doi:10.1016/j.compscitech.2017.06.006.

436 [7] A.E. Scott, I. Sinclair, S.M. Spearing, A. Thionnet, A.R. Bunsell, Composites : Part A

437 Damage accumulation in a carbon / epoxy composite : Comparison between a

438 multiscale model and computed tomography experimental results, Compos. Part A. 43

439 (2012) 1514–1522. doi:10.1016/j.compositesa.2012.03.011.

440 [8] S. Abrate, Impact on Laminated Composite Materials, Appl Mech Rev. 44 (1991) 155–

441 190.

442 [9] S. Georgiadis, A.J. Gunnion, R.S. Thomson, B.K. Cartwright, Bird-strike simulation for

443 certification of the Boeing 787 composite moveable trailing edge, Compos. Struct. 86

444 (2008) 258–268. doi:10.1016/j.compstruct.2008.03.025.

445 [10] G. Savage, I. Bomphray, M. Oxley, Exploiting the fracture properties of carbon fibre

446 composites to design lightweight energy absorbing structures, 11 (2004) 677–694.

447   doi:10.1016/j.engfailanal.2004.01.001.

448 [11] P.D. Soden, A.S. Kaddour, M.J. Hinton, Recommendations for designers and

449   researchers resulting from the world-wide failure exercise, Compos. Sci. Technol. 64

450   (2004) 589–604. doi:10.1016/s0266-3538(03)00228-8.

451 [12] M. Hinton, Failure Criteria in Fibre Reinforced Polymer Composites: Can any of the

452   Predictive Theories be Trusted, in: NAFEMS World Congr., Boston, 2011: p. 66.

453 [13] A. Kaddour, M. Hinton, Benchmarking of triaxial failure criteria for composite

454   laminates: Comparison between models of 'Part (A)' of 'WWFE-II,' 2012.

455   doi:10.1177/0021998312449887.

456 [14] A. Puck, H. Schurmann, Failure analysis of FRP laminates by means of physically based

457   phenomenological models, Compos. Sci. Technol. 58 (2002) 30.

458 [15] A. Puck, J. Kopp, M. Knops, Guidelines for the determination of the parameters in

459   Puck's action plane strength criterion, Compos. Sci. Technol. 62 (2002) 8.

460 [16] Y. Shi, C. Pinna, C. Soutis, Modelling impact damage in composite laminates: A

461   simulation of intra- and inter-laminar cracking, Compos. Struct. 114 (2014) 10–19.

462   doi:10.1016/j.compstruct.2014.03.052.

463 [17] C.G. Dávila, P.P. Camanho, C.A. Rose, Failure criteria for FRP laminates, J. Compos.

464   Mater. 39 (2005) 323–345. doi:10.1177/0021998305046452.

465   [18] P.P. Camanho, C.G. Dávila, S.T. Pinho, L. Iannucci, P. Robinson, Prediction of in situ

466   strengths and matrix cracking in composites under transverse tension and in-plane

467   shear, Compos. Part A Appl. Sci. Manuf. 37 (2006) 165–176.

468   doi:10.1016/j.compositesa.2005.04.023.

469   [19] S.T. Pinho, C.G. Dávila, P.P. Camanho, L. Iannucci, P. Robinson, Failure Models and

470   Criteria for FRP Under In-Plane or Three-Dimensional Stress States Including Shear

471   Non-linearity, Nasa/Tm-2005-213530. (2005) 68. doi:NASA/TM-2005-213530.

472   [20] H. Ghiasi, D. Pasini, L. Lessard, Optimum stacking sequence design of composite

473   materials Part I: Constant stiffness design, Compos. Struct. (2009).

474   doi:10.1016/j.compstruct.2009.01.006.

475   [21] P. Maimí, P.P. Camanho, J.A. Mayugo, C.G. Dávila, A continuum damage model for

476   composite laminates: Part II – Computational implementation and validation, Mech.

477   Mater. 39 (2007) 909–919. doi:10.1016/j.mechmat.2007.03.006.

478   [22] S. Eskandari, F.M. Andrade Pires, P.P. Camanho, A.T. Marques, Intralaminar damage in

479   polymer composites in the presence of finite fiber rotation: Part II – Numerical analysis

480   and validation, Compos. Struct. 151 (2016) 127–141.

481   doi:10.1016/j.compstruct.2016.01.048.

482   [23]   Scopus - Document search results on the composites damage modelling, last visited on

483   15th Oct, 2018, Https://Www.Scopus.Com. (2018).

484   [24]   D.M. Thomson, H. Cui, B. Erice, J. Hoffmann, J. Wiegand, N. Petrinic, Experimental and

485   numerical study of strain-rate effects on the IFF fracture angle using a new efficient

486   implementation of Puck's criterion, Compos. Struct. 181 (2017) 325–335.

487   doi:10.1016/j.compstruct.2017.08.084.

488   [25]   A. Puck, J. Kopp, M. Knops, Guidelines for the determination of the parameters in

489   Puck's action plane strength criterion, Compos. Sci. Technol. 62 (2002) 371–378.

490   doi:10.1016/S0266-3538(01)00202-0.

491   [26]   J. Wiegand, Constitutive modelling of composite materials under impact loading, PhD

492   thesis (2008).

493   [27]   J. Wiegand, N. Petrinic, B. Elliott, An algorithm for determination of the fracture angle

494   for the three-dimensional Puck matrix failure criterion for UD composites, Compos. Sci.

495   Technol. 68 (2008) 2511–2517. doi:10.1016/j.compscitech.2008.05.004.

496   [28]   S.T. Pinho, L. Iannucci, P. Robinson, Physically based failure models and criteria for

497   laminated fibre-reinforced composites with emphasis on fibre kinking. Part II: FE

498   implementation, Compos. Part A Appl. Sci. Manuf. 37 (2006) 766–777.

499   doi:10.1016/j.compositesa.2005.06.008.

500   [29]   P.P. Camanho, Failure Criteria for Fibre-Reinforced Polymer Composites, Demegi, Feup.

501   (2002) 1–13.

502   [30]   P. Maimí, D. Trias, E. V González, J. Renart, Nominal strength of quasi-brittle open hole

503   specimens,   Compos.   Sci.   Technol.   72   (2012)   1203–1208.

504   doi:10.1016/j.compscitech.2012.04.004.

505   [31]   H. Cui, D. Thomson, A. Pellegrino, J. Wiegand, N. Petrinic, Effect of strain rate and fibre

506   rotation on the in-plane shear response of ±45° laminates in tension and compression

507   tests,   Compos.   Sci.   Technol.   135   (2016)   106–115.

508   doi:10.1016/j.compscitech.2016.09.016.

509   [32]   H. Cui, A.R. Melro, M. Yasaee, Inter-fibre failure of through-thickness reinforced

510   laminates in combined transverse compression and shear load, Compos. Sci. Technol.

511   165 (2018) 48–57. doi:10.1016/j.compscitech.2018.06.011.

512   [33]   J. Hoffmann, H. Cui, N. Petrinic, Determination of the strain-energy release rate of a

513   composite laminate under high-rate tensile deformation in fibre direction, Compos. Sci.

514   Technol. 164 (2018) 110–119. doi:10.1016/j.compscitech.2018.05.034.

515   [34]   M. Ploeckl, P. Kuhn, J. Grosser, M. Wolfahrt, H. Koerber, A dynamic test methodology

516   for analyzing the strain-rate effect on the longitudinal compressive behavior of fiber-

517   reinforced   composites,   Compos.   Struct.   180   (2017)   429–438.

518   doi:10.1016/j.compstruct.2017.08.048.

519   [35] M.W. Czabaj, J.G. Ratcliffe, Comparison of intralaminar and interlaminar mode-I

520   fracture toughness of unidirectional IM7/8552 graphite/epoxy composite, NASA Tech.

521   Rep. (2012) 1–18. doi:https://doi.org/10.1016/j.compscitech.2013.09.008.

522   [36] H. Koerber, P.P. Camanho, High strain rate characterisation of unidirectional carbon–

523   epoxy IM7-8552 in longitudinal compression, Compos. Part A Appl. Sci. Manuf. 42

524   (2011) 462–470. doi:10.1016/j.compositesa.2011.01.002.

525   [37] H. Koerber, J. Xavier, P.P. Camanho, High strain rate characterisation of unidirectional

526   carbon-epoxy IM7-8552 in transverse compression and in-plane shear using digital

527   image correlation, Mech. Mater. 42 (2010) 1004–1019.

528   doi:10.1016/j.mechmat.2010.09.003.

529   [38] X. Xu, M.R. Wisnom, X. Sun, T. Rev, S.R. Hallett, Experimental determination of

530   Through-Thickness Compression (TTC) enhancement factor for Mode II fracture energy,

531   Compos. Sci. Technol. 165 (2018) 66–73. doi:10.1016/j.compscitech.2018.06.012.

532   [39] H. Cui, M. Yasaee, A.R. Melro, Dynamic inter-fibre failure of unidirectional composite

533   laminates with through-thickness reinforcement, Submitt. to Compos. Sci. Technol.

534   (2018).

535   [40] M.W. Czabaj, J.G. Ratcliffe, Comparison of intralaminar and interlaminar mode I

536   fracture toughnesses of a unidirectional IM7/8552 carbon/epoxy composite, Compos.

537   Sci. Technol. 89 (2013) 15–23. doi:10.1016/j.compscitech.2013.09.008.

538 [41] S.A. Ponnusami, H. Cui, M. Lißner, M. Pathan, B. Erice, An integrated numerical-

539   experimental approach to measure the dynamic Mode-I interlaminar fracture

540   toughness of fiber composites using wedge-DCB test and cohesive zone modelling,

541   Submitt. to Compos. Part B. (2018).

542 [42] M. Yasaee, G. Mohamed, A. Pellegrino, N. Petrinic, S.R. Hallett, Strain rate dependence

543   of mode II delamination resistance in through thickness reinforced laminated

544   composites, Int. J. Impact Eng. 107 (2017) 1–11. doi:10.1016/j.ijimpeng.2017.05.003.

545 [43] P. Kuhn, G. Catalanotti, J. Xavier, P.P. Camanho, H. Koerber, Fracture toughness and

546   crack resistance curves for fiber compressive failure mode in polymer composites

547   under high rate loading, Compos. Struct. 182 (2017) 164–175.

548   doi:10.1016/j.compstruct.2017.09.040.

549 [44] K.W. Gan, M.R. Wisnom, S.R. Hallett, Effect of high through-thickness compressive

550   stress on fibre direction tensile strength of carbon/epoxy composite laminates,

551   Compos. Sci. Technol. 90 (2014) 1–8. doi:10.1016/j.compscitech.2013.10.010.

552 [45] A. Hussien, M. Moehring, C. Schwall, B. Pipes, On Compressive Response of IM7/8552

553   Lamina- A Theoretical & Experimental Review, (2012). doi:10.2514/6.2012-1766.

554   [46]   J. Lee, C. Soutis, A study on the compressive strength of thick carbon fibre–epoxy

555   laminates, Compos. Sci. Technol. 67 (2007) 2015–2026.

556   doi:10.1016/j.compscitech.2006.12.001.

557   [47]   T.K. O'Brien, A.D. Chawan, R. Krueger, I.L. Paris, Transverse tension fatigue life

558   characterization through flexure testing of composite materials, Int. J. Fatigue. 24

559   (2002) 127–145. doi:10.1016/S0142-1123(01)00104-9.

560   [48]   R. Panduranga, K. Shivakumar, Mode-II total fatigue life model for unidirectional

561   IM7/8552 carbon/epoxy composite laminate, Int. J. Fatigue. 94 (2017) 97–109.

562   doi:10.1016/j.ijfatigue.2016.09.014.

563   [49]   G. Catalanotti, C. Furtado, T. Scalici, G. Pitarresi, F.P. van der Meer, P.P. Camanho, The

564   effect of through-thickness compressive stress on mode II interlaminar fracture

565   toughness, Compos. Struct. 182 (2017) 153–163.

566   doi:10.1016/j.compstruct.2017.09.014.

567   [50]   S.T. Pinho, P. Robinson, L. Iannucci, Fracture toughness of the tensile and compressive

568   fibre failure modes in laminated composites, Compos. Sci. Technol. 66 (2006) 2069–

569   2079. doi:10.1016/j.compscitech.2005.12.023.

570   [51]   H. Körber, Mechanical Response of Advanced Composites under High Strain Rates,

571   2010.

2019-01-25

A critical study on impact damage simulation of IM7/8552 composite laminate plate

Cui, Hao

Elsevier